Ultrafast excited state dynamics in the monomeric and trimeric Photosystem I core complex of *Spirulina platensis* probed by two-dimensional electronic spectroscopy

Mattia Russo[1,2], Anna Paola Casazza[3], Giulio Cerullo[1,2], Stefano Santabarbara[4] and Margherita Maiuri[1,2]**

[1]Dipartimento di Fisica, Politecnico di Milano, Piazza Leonardo da Vinci 32, 20133 Milano, Italy

[2]Istituto di Fotonica e Nanotecnologie del Consiglio Nazionale delle Ricerche, Piazza Leonardo da Vinci 32, 20133 Milano, Italy

[3]Istituto di Biologia e Biotecnologia Agraria, Consiglio Nazionale delle Ricerche, Via Bassini 15a, 20133 Milano, Italy

[4]PhotosynthesisResearch Unit, Centro studi sulla Biologia Cellulare e Molecolare delle Piante, Consiglio Nazionale delle Ricerche, Via Celoria 26, 20133 Milano, Italy

* corresponding authors:
Stefano Santabarbara stefano.santabarbara@cnr.it
Margherita Maiuri margherita.maiuri@polimi.it

ABSTRACT (250 words)

Photosystem I (PSI) is a naturally occurring supercomplex composed of a core part and a light-harvesting antenna, playing an essential role in the photosynthetic electron transfer chain. Evolutionary adaptation dictates a large variability in the type, number, arrangement and absorption of the Chlorophylls (Chls) responsible of the early steps of light-harvesting and charge separation. For example, the specific location of long-wavelength Chls (referred to as *red forms*) in the cyanobacterial core has been intensively investigated, but the assignment of the chromophores involved is still controversial. The most red-shifted Chl *a* form has been observed in the trimer of the PSI core of the cyanobacterium *Spirulina platensis*, with an absorption centred at ~740 nm. Here we apply two-dimensional electronic spectroscopy (2DES) to study

photoexcitation dynamics in isolated trimers and monomers of the PSI core of *Spirulina platensis*. By means of global analysis we resolve and compare direct downhill and uphill excitation energy transfer (EET) processes between the bulk Chls and the red forms, observing significant differences between the monomer, lacking the most far red Chl form at 740 nm, and the trimer, with the ultrafast EET component accelerated by 5 times, from 500 fs to 100fs, in the latter. Our findings highlight the complexity of EET dynamics occurring over a broad range of time constants, and their sensitivity to energy distribution and arrangement of the cofactors involved. The comparison of monomeric and trimeric forms, differing both in the antenna dimension and in the extent of red forms, enables us to extract significant information regarding PSI functionality.

I. INTRODUCTION

Photosystem I (PSI) is a key component of the photosynthetic electron transfer chain, catalysing the light-dependent oxidation and reduction of small water-soluble cofactor-proteins serving as electron shuttles: plastocyanin, or cytochrome c_6, at the donor side and ferredoxin, or flavodoxin, at the acceptor side[1]. Under functional and structural perspectives, PSI is considered to be composed of two moieties: a core complex and an external light-harvesting complement. The core complex is evolutionarily rather well conserved, although some species-dependent peculiarities are encountered, whereas the external antenna system varies considerably among organisms, as a result of adaption to specific ecological niches that in Nature can vary greatly in terms of both spectrum and flux of the incident light [2,3].

The conservation of the overall structural properties of the core complex can be rationalised considering that it is the site of photochemical energy conversion and its further stabilization through electron transfer reactions. Despite being composed of a variable number of protein subunits (11-15, depending on the species), most of the core-bound cofactors are coordinated by the two largest ones, called PsaA and PsaB, that form a hetero-dimer harbouring, almost ubiquitously, 88 – 96Chlorophyll (Chl) *a* and 22 β-carotene molecules, together with other cofactors involved in electron transfer reactions: 2 phylloquinone molecules and a [4Fe-4S] cluster, called F_X[4]. The largest difference in the overall core complex architecture between species is the monomeric

organization, found in eukaryotes, with respect to the dominant trimeric one (trimer of monomers) found in prokaryotic cyanobacteria even though, more recently, the occurrence of a tetrameric organization has also been reported in some species[5,6].Nonetheless, the trimeric form of the core complex appears to be the most widespread in this group of organisms, in which a dynamic reconfiguration between PSI core monomers and trimers might also occur to respond to environmental conditions[7,8]. The ability of forming trimers is linked to the presence of a specific subunit, PsaL, that is divergent in eukaryotes and, when deleted in prokaryotes, leads to PSI monomerization[9].

Of the large chromophore complement coordinated by each monomeric core complex, only six chlorins, that collectively compose the reaction centre (RC), participate to photochemical and electron transfer events. These chromophores are coordinated at the interface of the PsaA:PsaB hetero-dimer giving rise to an almost perfectly symmetric arrangement with respect to the symmetry axis perpendicular to the putative membrane plane in which the cofactor-protein supercomplex is embedded[10]. Of these six pigments, two are assigned to a Chl*a*:Chl*a*' dimer (the latter being an epimer), parallel to the symmetry axis and attributed to the terminal electron donor, referred to as $P_{700}^{(+)}$. The other four chlorins are organised as pseudo-dimers, each composed by the so-called eC_2 and eC_3 Chl *a* molecules, and each located at ~30° with mutual mirror symmetry with respect to the membrane plane. This arrangement gives rise to two close to identical electron transfer chains, one mainly coordinated by the PsaA and the other by the PsaB subunit, which however share P_{700} as a common cofactor, and later in the electron transfer cascade the iron-sulphur cluster F_X.

There is at present a general consensus that both cofactor chains are active in photochemical and electron transfer reactions[11,12]. The large number of cofactors bound to the core complex that do not participate in photochemistry and electron transfer processes, serves as a proximal light harvesting system to the RC. Yet, despite the overall similarity in the cofactor arrangement, the spectral properties of the core antenna Chls also show significant differences among species[2,13]. The most evident is that, whereas in eukaryotes, particularly in higher plants, long-wavelength Chl spectral forms are mostly coordinated by the external Light Harvesting Complex I (LHCI) antenna[14-17], in the case of prokaryotic cyanobacteria, these spectral forms are located in the core antenna instead[13,18,19]. Nonetheless, the exact transition energy and the

stoichiometric abundance of long wavelength Chl forms (often referred to as *red forms*) vary significantly in PSI core complexes isolated from different cyanobacteria, with band centres reported to fall in the 705 – 740 nm window and involving a number of Chl *a* varying from ~3 to 10 per core complex[13,18,19].

The red-shift in transition energy of these Chl forms is thought to arise from exciton coupling between two or more Chls and to correspond to the lowest exciton state within the cluster[13,18,19]. The specific location of long-wavelength Chls in cyanobacterial core has been intensively investigated but the assignment of the chromophores involved is still controversial[20-28]. Recent results indicate that excitons involving ChlsB37-B38 (nomenclature according to Jordan et al. crystallographic model[10]), B31-B32-B33 and B7-A31-A32 are responsible for the 710, 715 and 707 nm spectral red forms, at least in *Synechocystis sp.* PCC6803 and specific mutants of this species[29], although the general validity of this assignment has also been discussed by the authors. The most red-shifted Chl *a* form has, to our knowledge, been observed in the trimeric form of the PSI core of *Spirulina platensis*, with an absorption centred at ~740 nm and giving rise to an emission, mostly resolved at cryogenic temperatures, centred at 760 nm[13,30-38].

The role of red forms is to increase the absorption bandwidth in the far-red/near-infrared portion of the incident light spectrum, which can become significant especially under canopy shading/self-shading conditions[39]. Yet, their transition energy is lower than that of the pigments in the RC, implying a thermodynamically unfavourable excitation energy transfer (EET). This however was shown not to impact significantly on the overall PSI conversion quantum efficiency, which is estimated to always exceed 0.95, despite slowing down excited state equilibration in the antenna system[40-47]. The clearest evidence of kinetic limitations to the overall excited state equilibration is the progressive increase in excited state relaxation time towards the long wavelength emission tail, the extent of which depends both on the stoichiometry and specific red-form absorption. Thus, relaxation dynamics can be as much as five time slower in the red emission tail, *i.e.* about ~100 ps, than those observed for the bulk of Chl *a* forms absorbing at shorter wavelengths than the RC, *i.e.* ~ 20 ps[39]. This also results in excited state dynamics which depend on the site of initial excitation within the antenna matrix, being, in general, faster for excitation of "bulk" (short-wavelength absorbing) antenna Chls and slower upon direct excitation of the red forms. This was originally shown by

selective excitation experiments, at few specific wavelengths either by time-resolved fluorescence[48,49]or by transient absorption (TA)[50,51] measurements.

Two-Dimensional Electronic Spectroscopy (2DES) has the intrinsic ability to probe simultaneously, and therefore correlate, the site of initial excitation hidden underneath a large, spectrally broadened, absorption band, with the excited state dynamics through a wide spectral detection window[52,53]. Thanks to its high spectral selectivity, 2DES appears as particularly suited to study the effect of excited state dynamics in PSI allowing to probe, at the same time, the excited state dynamics upon photo-excitation in the bulk antenna Chls and in the red forms. Recently, a few 2DES studies have investigated the PSI-LHCI supercomplex[47,54] and the core complex[54] isolated from land plants, as well as core complexes isolated from different cyanobacteria, such as *Synechocystis sp.* PCC 6803, *Synechococcus sp.* PCC 7002[55]and *Thermosynechococcus elongatus*[56].

These studies focused primarily on the ultrafast processes, highlighting a very rapid transient (~20-50 fs) attributed to excited state delocalization among excitonically coupled Chls, and observed both downhill EET for bulk antenna Chls[56] and uphill EET involving the red forms present in these complexes[55].The occurrence of ultrafast energy redistribution among coupled pigments, not relying on exciton hopping, might play an important role in ensuring efficient energy equilibration within a large chromophore matrix, such as a photosystem antenna, especially in the case of long-wavelength absorption forms, for which hopping-based EET is energetically unfavourable. This spectroscopic approach has been very recently applied to mutants of *Synechocystis sp.* PCC 6803 having a reduced antenna size and low amount of Chl red forms[57]. Comparison of 2DES results acquired at room temperature and at 77 K, together with structure-based kinetic modelling, led to the suggestion of a charge separation occurring at a rate of 1.2−1.5 ps^{-1} [57], that is in line with the faster limit of previously reported photochemical rates[50,58], but proposed the occurrence of a bottleneck for effective trapping due to the EET from a pool of moderately red-shifted Chls, absorbing in the 685 – 695 nm range.

Although different in the exact content of long-wavelength Chl forms, all cyanobacterial cores investigated so far by 2DES harbour moderately red-shifted states, with transition energies in the 705 – 715 nm window. In this study, in order to further investigate the role of the red forms, we use 2DES to compare the dynamics of ultrafast EET processes in monomeric and trimeric PSI cores of *S. platensis*. The trimeric core

complex contains a very long wavelength form, with absorption maximum at ~740 nm[36,37], which is absent in the PSI monomers[13,35], thereby allowing an almost direct comparison. Nonetheless, the monomer still hosts the other less red-shifted spectral forms, characterized by transitions falling in the ~710-730 nm window for both forms of the complex[13,35-37]. Experiments were performed under conditions in which the terminal electron donor was pre-oxidised, *i.e.* in the cationic P_{700}^{+} state, in order to suppress electron transfer processes, which are known to kinetically overlap with the slow phases of EET in the tens of picoseconds time window[59].

Our results show the occurrence of ultrafast dynamics, followed by slower EET processes, which are significantly different, and display contrasting behaviour, in the trimeric and monomeric forms of *S. Platensis* PSI complex. In particular, ultrafast EET appears to be accelerated in the PSI trimers, with the faster resolved phase characterised by a lifetime of 100 fs, being about five time faster than in monomers. In trimers, this rapid phase also encompasses close-to-instantaneous excited state transfer from low-energy states (red forms) towards the bulk of the absorption, which is not compatible with incoherent excitation hopping. On the other hand, equilibration through downhill EET pathways between the bulk antenna and the red forms, which are further red-shifted in the trimers, shows slower components in this form of the complex. Moreover, the main relaxation taking place after the excited state has largely localised on the respective low energy states is about twice slower in trimers with respect to monomers. These observations highlight the complexity of EET dynamics occurring over a rather broad range of time constants, and their sensitivity to energy distribution and arrangement of the cofactors involved. The implications of these findings for our understanding of the functionality of the photosystem are discussed.

II. METHODS

A. Sample preparation

Trimeric and monomeric forms of *S. platensis* PSI were isolated as described by Shubin et al.[32]. For the measurement samples were suspended in 20 mM Tricine–NaOH pH 7.8, 100 mMKCl, 25 mM $MgCl_2$.

B. Steady-state absorption spectra

Absorption spectra were measured using a laboratory assembled spectrometer employing an OMA III (EG&G, model 1460) unit equipped with an intensified diode

array detector (Model 1420) mounted on a HR320 (Jobin-Ivon) spectrograph with a 150 groove mm^{-1} grating, giving a spectral resolution of 0.48 nm/pixel. The wavelength scale was calibrated using a neon lamp (Cathodeon). For absorption measurement the light source was a halogen lamp, connected to a custom built stabilised power supply, and filtered by a combination of neutral density and a long-pass filter with half-transmission at 510 nm. The detector was further protected by a long-pass filter (OG 530, Schott). The light path was 1 cm and the sample was diluted to give ~0.75 OD cm^{-1} at the absorption maximum.

C. Time-Correlated Single Photon Counting

Excited state fluorescence decay kinetics were detected using a laboratory assembled Time-Correlated Single Photon Counting (TCSPC) set-up. In brief, the excitation was provided by a pulsed diode laser (PicoQuant 800B) centred at 632 nm (FWHM 3 nm) and operating at a repetition rate of 20 MHz. The intensity (1 pJ per pulse) was sufficiently low to avoid non-linear absorption processes and build-up of long-lived metastable species. The emission wavelength was selected by a monochromator (CT-10, Jasco), after passing a polariser set at the magic angle (54.7°) to avoid distortions due to anisotropy decay. The emitted photons were collected by a cooled MCP photomultiplier (Hamamatsu, R5916U-51). The constant fraction discriminator, the time-to-amplitude converter and the storage of collected photon counts (4052 channels) were embedded within an integrated board (Becker & Hickl, SPC-330) mounted on a personal computer. Samples were placed in a 3 mm path-length cuvette and diluted to an optical density of 0.12 OD cm^{-1} at 680 nm to avoid spectral and kinetic distortions due to re-absorption. Sample temperature was 20°C with a circulating water bath (Lauda, RC5), and the sample chamber was flushed with nitrogen. To maintain the terminal donor in the oxidised state (P_{700}^{+}) potassium ferricyanide (2 mM) was added to the sample.

The decay of the excited state kinetics was analysed by a reiterative convolution of the 110 ps FWHM instrument response function (IRF), measured using a scattering solution (15% w/v Ficoll in 50 mM Hepes pH 7.5), and a decay model function, consisting of a weighted sum of exponential functions, using the global fit approach that considers the lifetimes (τ_i) as wavelength-independent parameters whereas the amplitudes ($A_i(\lambda)$) are unconstrained[60,61]. The plot of $A_i(\lambda)$ as a function of the emission wavelength yields the Decay Associated Spectra (DAS). Fits were performed

by a laboratory developed software[41] minimising the global reduced χ^2, through the MINUIT library from CERN, which also allows to analyse the confidence errors associated with the fit parameters.

The average and mean lifetimes, τ_{av} and τ_m, respectively, calculated from the global fit parameters are defined as: $\tau_{av}(\lambda) = \sum_i A_i(\lambda) \cdot \tau_i / \sum_i A_i(\lambda)$ and $\tau_m(\lambda) = \sum_i A_i(\lambda) \cdot \tau_i^2 / \sum_i A_i(\lambda) \cdot \tau_i$. Their respective values at the whole photosystem level are defined as: $\langle \tau_{av} \rangle = \sum_\lambda p(\lambda) \cdot \tau_{av}(\lambda)$ and $\langle \tau_m \rangle = \sum_\lambda p(\lambda) \cdot \tau_m(\lambda)$, where $p(\lambda) = \sum_i A_i(\lambda) \cdot \tau_i / \sum_{i,\lambda} A_i(\lambda) \cdot \tau_i$ is the (normalised $\sum_\lambda p(\lambda) \equiv 1$) probability of excited state residence at the observation wavelength, λ.

D. Two-Dimensional Electronic Spectroscopy

2DES exploits a sequence of three delayed laser pulses interacting with a sample that subsequently emits a third-order nonlinear signal as a function of the delays between the pulses. The first and the second pulse act as pump pulses and the delay between the two is labelled as t_1(coherence time). The third pulse acts as a probe and the delay between the second and the third laser pulse is referred to as population or waiting time, labelled as t_2. After the interaction of the third pulse, the emitted nonlinear signal, which follows at a time delay t_3 (detection time), is spectrally resolved by a spectrometer, which performs a Fourier transform providing the detection frequency axis. The excitation frequency axis is obtained by a further Fourier transform of the emitted signal with respect to the delay t_1, providing a 2D map which correlates excitation and detection frequencies for each value of the population time t_2. Details of the experimental apparatus adopted in this work can be found elsewhere[62]. Briefly, broadband laser pulses are generated by a home-made non-collinear optical parameter amplifier (NOPA) pumped by an amplified Ti:Sapphire laser (Coherent Libra) that emits 100-fs laser pulses centred at 800nm with 1-kHz repetition rate. The NOPA output spans 600-750nm and is temporally compressed with a pair of chirped mirrors to a nearly transform-limited duration. 2DES experiment are performed in a partially collinear configuration, which consists in a modification of a TA setup in which two phase-locked collinear pump pulses are generated by a birefringent interferometer, known as the Translating-Wedges-Based Identical pulses encoding System (TWINS)[63],

and combined with a non-collinear probe pulse. The nonlinear signal emitted from the sample, which is collinear with the transmitted probe (self-heterodyned configuration) is acquired by a spectrometer (Stresing Entwicklungsburo) that spectrally resolves the detection frequency axis. The overall temporal resolution of the 2DES setup is estimated to be better than 20 fs. Pump fluence was kept as low as 28 μJ/cm^2 and measurement conditions were analogous to those utilised in TCSPC experiments. The absence of significant contributions from non-linear annihilation processes was assessed by performing fluence-dependent experiments in a classical pump-probe configuration (Supplementary Information Figure S1). The samples were measured in a 200 μm fused silica cuvette with OD=0.3 at the absorption maximum. The measurements were performed by scanning t_2 delays from -250fs to 160ps.

III. RESULTS AND DISCUSSION

A. Fluorescence lifetimes of monomeric and trimeric PSI of *S. platensis*

The dynamics of excited state relaxation in monomeric and trimeric PSI of *S. platensis* under conditions in which the terminal electron donor P_{700} is pre-oxidised by ferricyanide were investigated by TCSPC. The results of global fitting of the fluorescence decay traces over the 675–785 nm window, in 10 nm steps, are reported as DAS in Figures 1a and 1b, for PSI monomers and trimers, respectively. In both cases the decay is satisfactorily described by four exponentials, characterised by lifetimes of 5.9, 19.2, 54.5, and 824 ps in the case of monomers, and 5.5, 37.0, 53.6 and 840 ps in the case of trimers. Hence, the values of lifetimes do not differ significantly between the two oligomeric states of the complex, except for the intermediate component of 19.2 ps in monomers which increases to 37 ps in trimers. These values are in fair agreement with those previously reported under "open" (P_{700} in its ground, neutral, state) conditions[13,34]. Faster components (<5 ps) were resolved by streak camera detection that has superior temporal resolution with respect to TCSPC[48], and are collectively described here by the fastest ~5 ps lifetime which is already close to the limit of temporal resolution of the set-up employed in this study (sub-ps kinetics will be addressed further below by 2DES spectroscopy). The slowest dynamics resolved by TCSPC has a very small amplitude. In accordance with previous studies[34] this is

attributed to an almost negligible amount of impurities, *i.e.* residual PSII core complexes or disconnected Chls and will not be discussed further.

Although the values of the lifetimes do not change greatly between *S. platensis* PSI monomers and trimers, some differences are instead present in the DAS spectral shape, particularly concerning the intermediate component of 19.2 ps in monomers and 37.0 ps in trimers. To interpret the DAS spectra extracted from the global analysis, one should recall that a positive amplitude represents a decay process, while a negative amplitude describes a excited state population transfer (signal rise). Both in PSI monomers and trimers the ~ 5 ps lifetimes includes contribution associated to EET from short wavelength to long wavelength Chl forms, corresponding to the negative DAS amplitudes. Yet, in both cases these DAS are not fully conservative (i.e., the integrated area is not zero), indicating that excited state relaxation of short-wavelength Chl *a* antenna forms is already taking place on this time scale. In PSI monomers the 19.2 ps and the 54.5 ps DAS have positive amplitude over the entire emission window, with the former (19.2 ps) having the largest amplitude and the latter (54.5 ps), although of lower amplitude, being further red-shifted. Hence, the 54.5 ps DAS is dominated by the decay of the lowest energy states in the monomeric core antenna.

In PSI trimers the 53.6 ps component is instead the dominant one, being the only DAS with fully positive amplitude. The 53.6 ps DAS in trimers shows an even more pronounced spectral red-shift with respect to PSI monomers, being dominated by an emission form centred at ~ 740 nm, and accompanied by an intense shoulder centred at ~715-720 nm that is also visible in the 54.5 ps DAS of the monomers. The 37.0 ps DAS of the trimers shows some EET features, having positive amplitude below 730 – 735 nm, with a maximum at ~715 nm, and negative amplitudes in the long-wavelength emission tail. It therefore likely contains contributions arising from relatively slow excited state equilibration between some of the moderately red-shifted Chl forms and the lowest energy states in the core antenna.

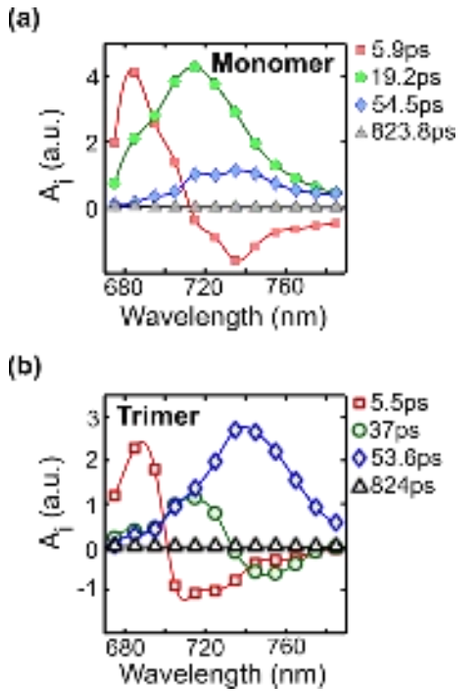

Figure 1. Decay Associated Spectra (DAS), resulting from global analysis of TCSPC kinetics in monomeric (a) and trimeric (b) PSI of *S. platensis*, at room temperature and with pre-oxidised P_{700} . (a): lifetimes 5.9 ps (red solid squares), 19.2 ps (green solid circles), 54.5 ps (blue solid diamonds), and 823.8ps (black solid triangles) (b): 5.5 ps (red open squares), 37 ps (green open circles), 53.6 ps (blue open diamonds), 840 ps (black open triangles). DAS spectra are normalised to the respective integrated steady-state emission in the investigated window.

Estimating the average lifetime over the whole emission bands $\langle \tau_{av} \rangle$, values of 32.7 ps and 65.6ps are obtained for PSI monomers and trimers, respectively, whereas for the mean lifetime $\langle \tau_m \rangle$, these values are 33.9 ps and 51.6ps, respectively. Thus, whereas it is apparent that the presence of further red-shifted Chl forms in the antenna of PSI trimers does slow down the excited state relaxation by a factor of ~1.5–2, at the whole photosystem level, these relaxation kinetics remain fast and largely comparable with those observed for active photochemical trapping, also under conditions in which P_{700} is pre-oxidised and the formation of stable radical pair states by electron transfer is prevented.

This observation, which agrees with previous reports[47,59,64], allows us to study the excited state dynamics under conditions which are relevant for the fully functional state of the complex, but which are simplified under the kinetic perspective, as electron transfer and EET processes overlap both temporally and spectrally, therefore complicating the interpretation of experimental data. Thus, in the following, EET

dynamics in the monomeric and trimeric PSI of *S. platensis* will be further investigated by 2DES spectroscopy under closed RC conditions, i.e. in the absence of stable radical pair formation.

B. 2DES spectroscopy of *S. platensis* PSI monomers

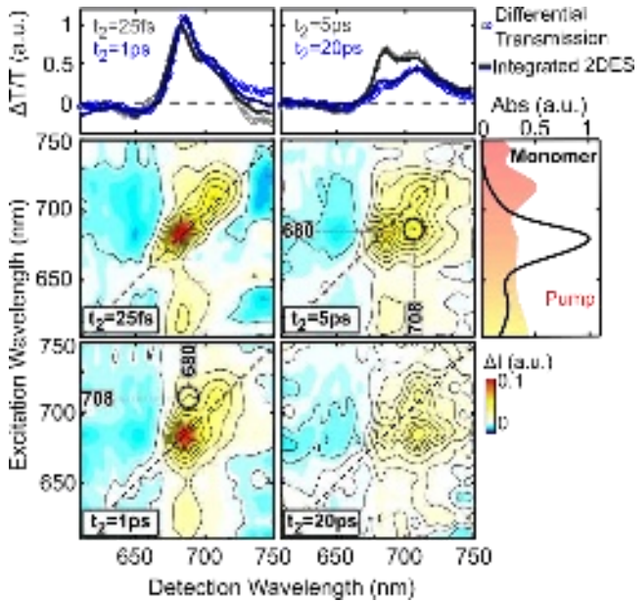

Figure 2 Purely absorptive 2DES maps of*S. Platensis*PSI monomers at t_2: 25fs, 1ps, 5ps and 20ps; top panels display the 2DES maps integrated along the excitation wavelength axis (continuous lines) compared with TA spectra (symbols) measured at the same delays; the right panel shows the static absorption spectrum of the sample measured at room temperatureoverlapped with the pump spectrum.

Figure 2 shows the purely absorptive 2DES maps of the monomeric form of *S. Platensis* PSI at t_2=25 fs, 1 ps, 5 ps and 20 ps; the upper panels show a comparison between the 2DES maps integrated along the excitation wavelength axis and the TA spectra acquired at the same waiting times. At t_2=25 fs, the positive signal of the 2DES map is mainly located along the diagonal where two peaks are visible; one centred at 680nm, corresponding to the Ground State Bleaching (GSB) signal of the Q_y band of Chl *a* molecules comprising the bulk of the photosystem antenna and the other at 708nm which is the GSB signal of Chl red forms. The main GBS features in the 2DES map correspond nicely to the peaks observed in the steady-state absorption spectrum reported on the right panel of Figure 2. At early times, the map shows a cross peak corresponding to excitation at 620 nm and detection at 680 nm. These wavelengths correspond to (unselective) excitation of the vibrational overtones of the Q_y band as well as the the Q_x bands of Chl *a,* and detection at the maximum of antenna absorption. Such a cross peak reveals an ultrafast energy equilibration process from the vibrational replicas of the Q_y and the Q_x band to the main (0-0) Q_y band of Chl *a* molecules of the

"bulk" antenna. Although part of this component can be ascribed to intra-molecular energy transfer, the cross peak at 680 nm indicates also EET from short-wavelength Chl forms, absorbing in the 660 – 675 nm window, whose presence is clear in the steady-state absorption spectrum (Figure 2 right panel), to the 680 nm Chl forms. At t_2=1 ps the lineshape of the diagonal peak at 680nm changes from elliptical (at t_2=25 fs) to circular due to spectral diffusion[65]. Furthermore, a cross peak corresponding to excitation at 708 nm and detection at 680 nm (emphasized in the 2DES map with a dashed circle) is observed, which suggests possible coupling between Chl red forms and bulk Chls. At t_2=5 ps the 2DES map shows the formation of a cross peak corresponding to excitation at 680nm and detection at 708 nm (again emphasized with a dashed circle), representing a downhill EET from the bulk Chls to the red forms. At t_2=20 ps the signal is mainly located around 710 nm detection wavelength, where the Chl red forms absorb.

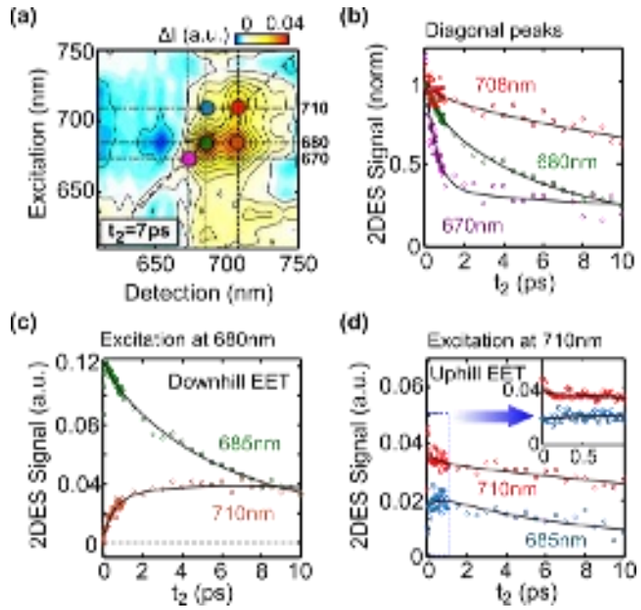

Figure 3 2DES dynamics of *S.platensis*PSI monomers: (a) purely absorptive 2DES map at t_2=7ps; black dashed lines correspond to the following excitation/detection wavelengths: 670nm, 680nm and 710nm and the colored circles correspond to the following excitation/detection points: 670/670nm (violet), 680/680nm (green), 710/710 nm (red), 680/710nm (orange) and 710/680nm (light blue); (b) temporal traces of the three diagonal peaks indicated in panel (a); (c) temporal traces corresponding to excitation at 680nm and detection at 685nm (green) and 710 nm (orange); (d) temporal traces corresponding to excitation at 710nm and detection at 685nm (light blue) and 710nm (red); the same dynamics zoomed on the 1-ps timescale is reported on the top-right as an inset. In panels (b), (c) and (d) the experimental data (colored circles) are overlapped with the best fit (continuous black lines) obtained by global analysis. In panels b-d only the dynamics up to 10 ps are shown to highlight ultrafast processes (see Figure S2 of the supplementary information for dynamics over the full acquisition window).

The temporal evolution of the EET processes between the bulk Chls and the red forms is reported in Figure 3, in which the experimental data (colored points) and the best fits (continuous black lines) of the dynamics are reported. Figure 3a shows the purely

absorptive 2DES map of the monomeric form at t_2=7 ps, where three diagonal peaks at 670nm (high energy bulk Chls), 680nm (Q_y band of bulk Chls) and 708nm (main absorption of Chl red forms) are emphasized with colored dots. Figure 3b shows the normalized dynamics of the diagonal points in which it is possible to distinguish three different decays for each excited state Chl pool; specifically, the decay is clearly faster for the bulk Chls and slower for the red forms, in agreement with previous observations[34,48] and with the TCSPC data of Figure 1. The EET between different Chl pools can be better identified by the dynamics of the cross peaks. Figure 3c shows the dynamics of the peaks measured by exciting at 680 nm and detecting at 685 nm (low energy Q_y state of bulk Chls) and 710 nm (orange point in Figure 3a). Such dynamics show a decay of the bulk Chls signal (green) and a simultaneous build-up of Chl red forms, representing the downhill EET between these states. Figure 3d shows the dynamics obtained by exciting the system at 710 nm (absorption of Chl red forms) and detecting at 710 nm and 685 nm (blue point in Figure 3a). In this case, both dynamics show a long decay (>10 ps), but the main difference appears on the 1-ps time scale. For this reason, a zoom of this time range is reported in the same plot as an inset. In this time scale the dynamics detected at 710 nm shows an ultrafast decay matching with the rapid formation of the signal detected at 685 nm. The best fits shown in Figures 3b, c and d (continuous black lines), are obtained from a global analysis algorithm in which the entire 2DES data set is modeled with a linear combination of exponential decays. The final result of this analysis can be expressed with a series of two-dimensional maps that represent the amplitude of each exponential decay. These maps are called two-dimensional Decay Associated Spectra (2D-DAS) and the sign of the amplitude and the corresponding time constant allow to characterize the different evolving processes spectrally and temporally. As for the TCSPC global analysis, here positive amplitude represents a GSB decay process, while the negative amplitude describes a formation mechanism[66]. 2DES data of *S. platensis* monomeric PSI, over the full dynamic range investigated (20 fs- 160 ps), are satisfactorily described by four exponentials characterized by lifetimes of: τ_1=520±30 fs, τ_2=5.4 ±0.2 ps, τ_3=30± 1 ps and a non-decaying component (τ_4>>160 ps). Figure 4 shows the first three 2D-DAS together with the retrieved time constants whereas the fourth component is reported in the Supporting Information (Figure S5a) because it is of very low amplitude and is largely dominated by scattering contributions. It can therefore be neglected in the data interpretation. Furthermore, a constrained global analysis model with the first DAS component fixed

at 100 fs was also tested (Figure S5b). This component corresponds to the fastest reliable lifetime resolvable through the employed set-up, and was instead clearly resolved in *S. platensis* PSI trimers (vide infra Section C). The constrained analysis of PSI monomer resulted however in a much lower fit quality, particularly in the sub-picosecond time window, as shown for selected dynamics reported in Figure S6 for the free (Figure S6(a)) and constrained (Figure S6(b)) models.

The lifetimes obtained from the global fits of 2DES maps are in fair agreement with those resolved by TCSPC (Section IIIA). However, 2DES resolves a sub-ps component that is not accessible by TCSPC, whereas the latter resolves a longer-lived component (~50 ps) which is not clearly observed in 2DES global fitting. The τ_3= 30 ps time constant obtained by 2DES thus most likely corresponds to an average of the 19.2 ps and 54.5 ps lifetimes retrieved by TCSPC. The similarity of overall relaxation times obtained by the two methods indicates substantial absence of non-linear relaxation processes (mainly singlet-singlet annihilation) in the 2DES measurements, that would give rise to an acceleration of the excited state decay.

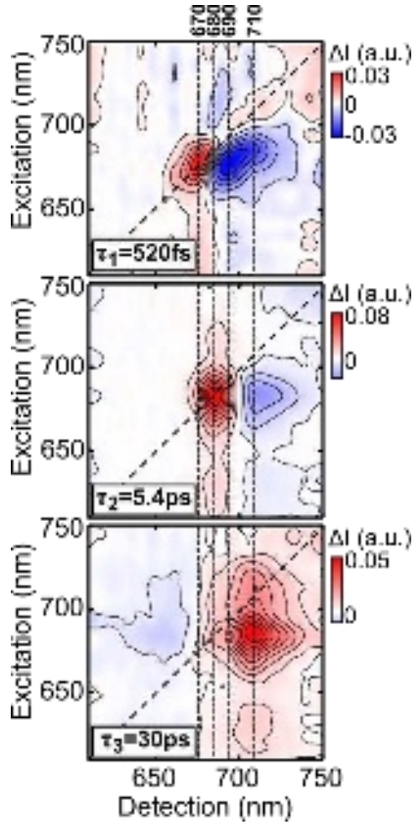

Figure 4 Global analysis results of *S.platensis* PSI monomers: 2D-DAS maps associated with the following time constants (from the top): τ_1=520 ± 30 fs, τ_2=5.4 ± 0.2 ps and τ_3=30 ± 1 ps; vertical black dashed lines are used to emphasize the following detection wavelengths: 670nm, 680nm, 690nm and 710nm. The non-decaying component is shown in Figure S5 of the supplementary information)

The first 2D-DAS (τ_1=520 fs) shows two processes: a decay (positive, red in Figure 4) at 670/670 nm excitation/detection wavelengths and a formation (negative, blue in Figure 4) at 670/690 nm excitation/detection wavelengths. This behavior represents mainly an energy equilibration within bulk Chls. Interestingly, some ultrafast (energetically downhill) EET to the red forms (>700 nm) is already present in the 520-fs DAS. Furthermore, by looking at the red forms spectral region (700 – 730 nm), the 2D-DAS shows a positive band at the diagonal peak, accompanied by a negative cross peak detected at 685 nm, which corresponds to the absorption tail of the Q_y band of bulk Chls. Such a process can be interpreted as an ultrafast uphill EET, as discussed for the dynamics of Figure 3d. The second 2D-DAS has a time constant of 5.4 ps, showing decay of a diagonal peak at 680nm and formation of a cross peak in the 700 – 730nm spectral region. This component thus contains significant contributions of EET from bulk Chls toward the red forms. The temporal evolution of this process is shown clearly in the dynamics reported in Figure 3c. However, this 2D-DAS is not purely conservative, as positive amplitudes observed over the bulk Chls are larger than the negative ones over the long wavelength absorption tail. Thus, together with EET to the red-states, also important contributions associated to the relaxation of the bulk Chls are already present in the 5 ps 2D-DAS, in good agreement with what observed in TCSPC data analysis (Figure 1). The temporal overlap of excited state relaxation and ETT explains the non-conservative nature of this component. It is possible that the two processes occur with similar, yet not identical, dynamics, and that also show some kinetic dispersion[45,50,51,67,68]. Closely spaced, and distributed, components would then be hardly resolvable when considering only a limited number of exponential decays. Finally, the third 2D-DAS of 30 ps describes the decay of the cross peak at 700 – 730 nm detection region, and corresponds to the relaxation of Chl red forms, that is clearly slower with respect to that of the bulk antenna.

C. 2DES spectroscopy of *S. platensis* PSI trimers

Figure 5 shows the purely absorptive 2DES maps of the trimeric PSI of *S. platensis* at t_2=25 fs, 1 ps, 5 ps and 20 ps. The comparison between the TA spectra (symbols) and the excitation wavelength integrated 2DES maps is reported on the top and the steady-state absorption spectrum on the right. At t_2=25 fs, the 2DES map shows two strong signals along the diagonal which correspond to the GSB of the Q_y band of Chls *a* (680 nm) and Chl red forms (>710 nm). With respect to its monomeric form, the trimer

exhibits a broader and red shifted absorption of the Chl red forms[48]. A weak but unambiguous cross peak corresponding to the bulk antenna absorption (680– 690 nm) upon pumping at wavelength >705 nm is already discernible at 25 fs delay, indicating an ultrafast energy redistribution from the red forms to part of the bulk antenna.

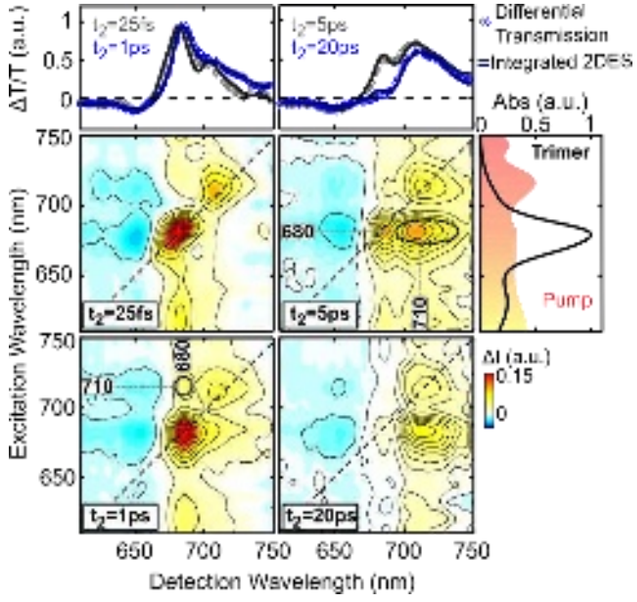

Figure 5 Purely absorptive 2DES maps of Spirulina PSI Trimers at t_2: 25fs, 1ps, 5ps and 20ps; top panels display the 2DES maps integrated along the excitation wavelength axis (continuous lines) compared with TA spectra (symbols) measured at the same delays; the right panel shows the static absorption spectrum of the sample measured at room temperature overlapped with the pump spectrum.

In the 2DES map recorded at a t_2=1 ps, the diagonal peak centered at 680 nm shows a lineshape elongation along the excitation wavelength axis due to an energy equilibration process within Q_y band of bulk Chls[56]. Furthermore, the formation of a cross peak at 710/680 nm excitation/detection wavelength (emphasized with a dashed circle) is also observed, representing an uphill EET processes as for the case of the monomer. At t_2=5 ps the 2DES map shows broad cross peaks by exciting at 680nm and detecting in the 700 – 740 nm spectral band (emphasized with a dashed ellipse). This signal is broader with respect to the monomeric form and it corresponds to a superposition of at least two Chl red forms, with absorption centered at ~710 nm and at ~ 730 nm, respectively. At t_2=20 ps the system shows a weak GSB signal of bulk Chls, whereas the excited state population appears to be localized almost entirely on the red forms.

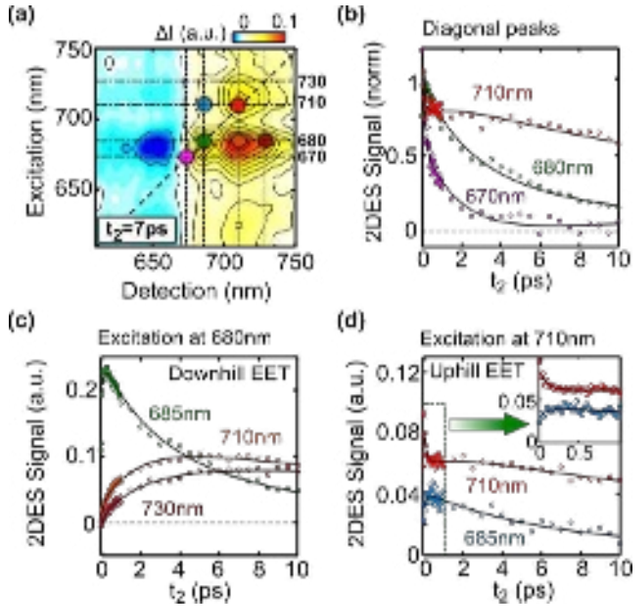

Figure 6 2DES dynamics of *S. platensis* PSI Trimers: (a) purely absorptive 2DES spectrum at t_2=7ps in which the black dashed lines correspond to the following excitation/detection wavelengths: 670nm, 680nm, 710nm and 730nm and the colored circles correspond to the following excitation/detection points: 670/670nm (violet), 680/680nm (green), 710/710 nm (red), 680/710nm (orange), 680/730nm (dark red) and 710/680nm (light blue); (b) temporal traces of the three diagonal peaks indicated in panel (a); (c) temporal traces corresponding to excitation at 680nm and detection at 685nm (green), 710 nm (orange) and 730nm (dark red); (d) temporal traces obtained by exciting at 710nm and detecting at 685nm (light blue) and 710nm (red); the same dynamics zoomed on the 1-ps timescale is reported on the top-right as an inset. In panels (b), (c) and (d) the experimental data (colored circles) are overlapped with the best fit (continuum black lines) obtained using global analysis.. In panels b-d only the dynamics up to 10 ps are shown to highlight ultrafast processes (see Figure S3 of the supplementary information for full dynamic window)

Figure 6a shows the purely absorptive 2DES map at t_2=7 ps of the trimeric form of *S. platensis* PSI, gridded with black dashed lines at selected, characteristic, wavelengths (670 nm, 680 nm, 710 nm and 730 nm). Figure 6b shows the normalized dynamics of the diagonal peaks at 670 nm (violet), 680 nm (green) and 710 nm (red) together with the best fit obtained with the global analysis (continuous lines). The dynamics associated with the excited states of bulk Chls (670 and 680 nm) show an exponential decay, however the dynamics of the diagonal peak associated with Chl red forms (710 nm) shows a combination of decay and formation, clearly distinct from the one of monomeric PSI (Figure 3b). Figure 6c shows the dynamics of the excitation/detection points at 680nm/685nm (Bulk Chls), 680 nm/710 nm and 680 nm/730 nm (red forms). From these data we note that: (i) the dynamics detected at 685 nm shows a fast formation due to the energy equilibration process within the bulk Chls; (ii) the dynamics detected at 710 nm and 730 nm refer to the downhill EET from the bulk Chls to the red forms; (iii) the dynamics detected at 730 nm shows a formation which is slower with respect to the one detected at 710 nm.

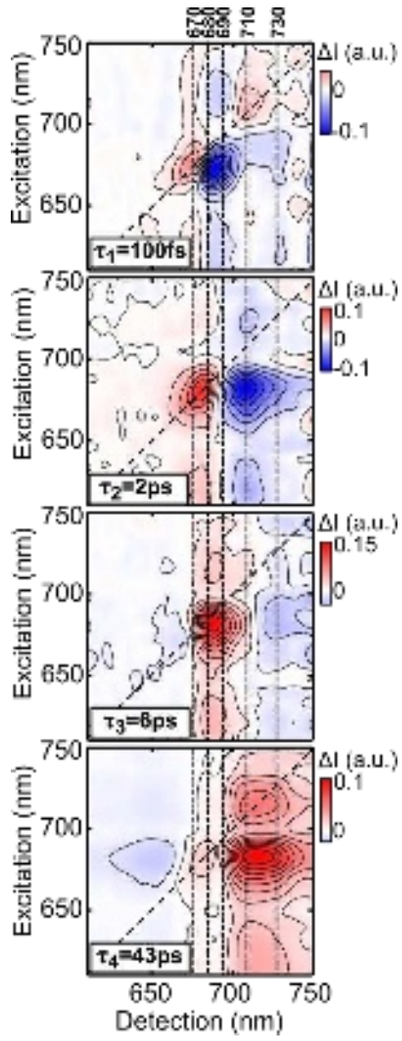

Figure 7 Global analysis results for *S. platensis*PSI Trimer: 2D-DAS maps associated with the following time constants (from the top): τ_1=100± 30 fs, τ_2=2± 0.2 ps, τ_3=6± 0.2 ps and τ_4=43 ± 1 ps; vertical black dashed lines are used to emphasize the following detection wavelengths: 670nm, 680nm, 690nm, 710nm and 730nm.

The occurrence of an uphill EET process from the red forms to the bulk is also observed in the trimeric PSI of *S. platensis*, as already noticed for the monomeric form of the complex. Figure 6d shows the dynamics of the 710 nm/710 nm and 710 nm/685 nm excitation/detection wavelength correlations and their temporal evolution up to 1ps is reported in the same plot as an inset. In this case the sub-500-fs decay of the Chl red forms (red curve) is accompanied by the fast formation of a signal at 685nm (uphill EET). For time delays longer than 1ps, the dynamics of the cross peak is faster with respect to the lifetime of the red forms, as observed by the diagonal peak at 710 nm.

The best fit of the 2DES data in PSI trimers is obtained by a linear combination of four exponential decays. The quality of the fit is shown by the continuous lines at selected excitation/detection wavelengths in Figure 6 and the complete 2D-DAS are reported in Figure 7. As for the case of the monomers, the lifetimes are in fair agreement

with those obtained by TCSPC (Section IIIA, Figure 1b), but further detail is obtained from 2DES for ultrafast processes, whereas slower relaxation dynamics are collectively described by a single component in the 2D-DAS. The first 2D-DAS exhibits a time constant of τ_1=100±30 fs and the positions of the maximal positive and negative amplitudes are similar with respect to the first 2D-DAS of the monomeric case.

The main difference between the two PSI superstructures is the value of τ_1 since the energy equilibration and the uphill EET processes are almost *five time faster* in the trimer with respect to the monomer. This is particularly obvious also for the uphill EET from red forms (centred at ~710 nm) to the low energy forms of the bulk (~685 – 690 nm). A plot comparing the temporal traces for the trimer and the monomer in the sub-picosecond window is presented in Figure S4, where the differences in the kinetics of signal rise (690 nm) and decay (675 nm) between the two oligomeric states of PSI can be directly appreciated.

However, the 100-fs 2D-DAS of trimers appears to be largely non-conservative, with dominant traits corresponding to the Chl pool to which energy is transferred (i.e. negative amplitudes). Yet, the retrieved lifetime is in this case close to the instrumental temporal resolution, since convolution with the instrumental response function was not included in the analysis. Therefore, both the exact lifetime values and the corresponding amplitudes have larger associated statistical uncertainties, which may lead to spectral distortions. This is most likely the reason for the largely non-conservative amplitudes in the 100-fs 2D-DAS, that might also stem from some even faster processes involving bulk Chls centred at ~680 nm which remain unresolved, leading to an apparent amplitude loss in this spectral window.

Noteworthy, ultrafast uphill EET has been already reported in the trimeric PSI of *Synechocystis sp.* PCC 6803 and *Synechococcus sp.* PCC 7002[55,57]. As previously noted, the lifetime of ~100 fs is on the edge of the estimated hopping time for incoherent EET. The observation of a clear cross-peak at wavelength <690 nm upon excitation in the red absorbing tail at 25 fs delay, suggests that the fastest process involves also transfer mediated by strong excitonic interactions, therefore likely involving coherent mechanisms. One such process might likely be excited state redistribution within an excitonically coupled Chl cluster/domain.

The second 2D-DAS has a lifetime of τ_2=2± 0.2 ps and the positive/negative amplitude are peaked at 685 nm/710 nm detection wavelength. It is worth to note that in this case the positive and negative peaks have the same amplitude, suggesting that

downhill EET from the bulk to the Chl red forms is the dominant process. This component does not have a clear correspondence in the monomeric PSI. It is possible that the 520-fs 2D-DAS observed in the monomers represents a weighted average of the 100-fs and 2-ps phases observed in trimers. These two phases cannot however be discerned even upon increasing the number of exponentials in an unconstrained analysis of monomeric PSI data, whereas a constrained analysis forcing a resolution-limited lifetime led to a lower fit quality (Figures S5b and S6b). This suggests that in monomers, if present, the two fast ETT phases are likely both more closely spaced in the lifetime space and less spectrally distinct.

The third 2D-DAS in *S. platensis* PSI trimers shows a time constant of τ_3=6 ± 0.2 ps, and is dominated by the decay of the signal associated with bulk Chls, detected at 680 nm. A similar time constant was obtained also for the monomeric structure in which the relaxation time of bulk Chls was 5.4 ps. This 2D-DAS also shows a weak negative amplitude detected at 730 nm which corresponds to a EET channel from the bulk Chls to low-energy Chls centred at 730 nm. This relatively slow EET also manifests itself directly in the kinetics (Figure 6c). The lack of conservation between areas of positive and negative amplitudes of the 6-ps 2D-DAS, is, as already discussed for the 5.4-ps 2D-DAS observed in monomers (Figure 4), then explained by the largely overlapped dynamics of relaxation of bulk Chls to the ground state and EET from the bulk Chls to the Red forms. Yet, these processes show uneven contributions to the 5-6 ps 2D-DAS, since the dominant amplitudes are the positive ones, centred around 680 nm detection wavelength that corresponds to the maximal (linear) absorption. The amplitude asymmetry is larger in trimers than monomers. Yet, in both cases, excited state relaxation of the bulk antenna is the dominant process assignable to the kinetic phase occurring in 5-6 ps.

Finally, the last 2D-DAS is associated with a time constant of τ_4=43± 1ps and it is dominated by the relaxation of Chls red forms in the 705 – 740 nm spectral range. The value of this lifetime is about twice as long as the one retrieved in the monomers, indicating that the extension of the absorption spectrum to the near-infrared is accompanied by sizable slowing down of the overall excited state relaxation, as also shown by TCSPC.

IV. CONCLUSIONS

In this work, we applied 2DES to investigate the energy equilibration and EET processes in monomeric and trimeric PSI of *Spirulina platensis*. Measurements were performed under conditions of pre-oxidised P_{700}, hence preventing the population of stable radical pairs. It is worth noting that EET to the non pre-oxidised chromophores composing the reaction centre, i.e. the so-called eC2/eC3 Chls, is still possible under these conditions. Yet, these molecules could be considered, within a first order approximation, to be components of the bulk antenna. This assumption is justified by the absence of a dynamic component that can unambiguously be associated to EET from the antenna to the reaction centre under the measurement conditions employed in this study. Therefore, EET and (non-photochemical) excited state relaxation are the dominant, if not the exclusive, processes. A complete spectral and temporal characterization was performed by analysing the experimental data of both PSI oligomeric states with global analysis in which the dynamics is described by a series of exponential decays. Figure 8 shows a diagram summarising the principal energy deactivation pathways of both systems (monomer on the left and trimer on the right), in which the estimated time constant of each process was obtained from the global analysis results. In monomers, only one ultrafast process comprising energy equilibration within the bulk Chls and uphill EET from the Chl red forms to Chls of the bulk is resolved, and it is characterised by the lifetime, τ_1=520 fsThe sub-ps EET processes are followed by the downhill EET from bulk Chls to red forms that overlaps kinetically to the relaxation of the bulk Chls to the ground state (τ_2=5.4 ps). The Chl red forms then relax to the ground state with the slowest detected time constant, (τ_3=30 ps.

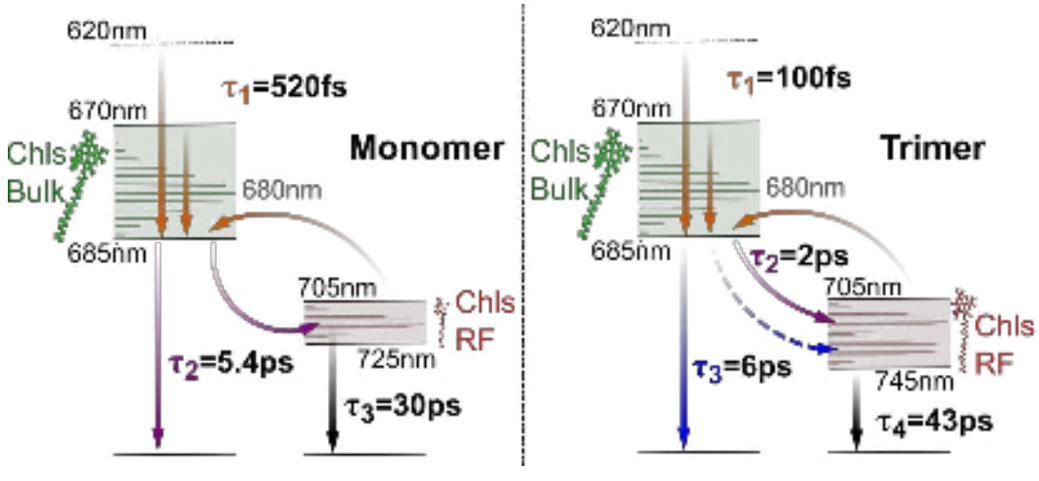

Figure 8 Energy level schemes of *S. platensis* PSI monomers (left) and PSI trimers (right) and deactivation pathways obtained from a global analysis of the 2DES data. For the PSI monomer, the temporal evolution of the system can be described by three time constants: τ_1=520fs (orange arrows) represents an intraband

transition of bulk Chls and an uphill EET from Chl red forms to bulk Chls, τ_2=5.4ps (violet arrows) represents a downhill EET from bulk Chls to Chl red forms and the relaxation of bulk Chls, τ_3=30ps (black arrow) represents the relaxation of Chl red forms. For the PSI trimer, the temporal evolution of the system can be described with four time constants: τ_1=100fs (orange arrows) represents an intraband relaxation of bulk Chls and an uphill EET from Chl red forms to bulk Chls, τ_2=2ps (violet arrow) represents a downhill EET from bulk Chls to Chl red forms, whose absorption is peaked around 715nm, τ_3=6ps (blue arrows) represents the relaxation of bulk Chls and a weak EET from bulk Chls to low-energy Chl red forms (dashed blue arrow), whose absorption is peaked around 730nm, τ_4=43ps (black arrow) represents the relaxation of Chl red forms.

The deactivation energy level scheme for the comparative analysis performed in PSI trimers is reported on the right side of Figure 8. In this case energy equilibration within bulk Chls and uphill EET are five times faster (τ_1=100±30 ps fs) with respect to the quickest resolvable EET process in monomers. The increase in the rate of both downhill and uphill EET observed in the trimer is not trivial since, in principle, the increase in the antenna dimension should have the opposite effect, or have only a moderate one, considering that the number of nearest neighbor pigments remains largely unchanged for most chromophores, with the exception of those located at the monomer-monomer interface. Our data therefore suggest that the specific interactions, established upon trimer formation, facilitate energy diffusion through the whole extended antenna network. At the same time this would imply that at least some red forms are located at the monomer-monomer interface, or at least on the outskirt of the single monomer antenna. It is not possible to completely rule out the occurrence of ultrafast EET also in monomers, but this could not be unambiguously resolved. If different, closely spaced, EET processes were to occur in monomers, the experimentally retrieved 520-fs lifetime should be considered to represent their weighted average.

The second process identified from the experimental data in PSI trimers is an almost pure downhill EET from bulk Chls to Chl red forms (τ_2=2 ps) which is distinguishable from the relaxation mechanism of the bulk Chls to the ground state (τ_3=6 ps). These two processes were almost indistinguishable in the monomers, being described by a single lifetime of ~5.5 ps. This indicated that, whereas the main de-excitation from the bulk Chls proceeds with about the same rate in monomers and trimers, energy transfer to the moderately red-shifted Chls is faster in the trimer with respect to the monomer, and becomes thus discernable. Yet, in the 6 ps 2D-DAS of PSI trimers (Figure 7), the presence of a negative amplitude in the spectral region above 725 nm is also observed, ascribed to further downhill EET from bulk Chls to the Chl red forms (absorption peak at 730 nm). This suggests a gradient of excited state equilibration, which becomes progressively slower towards the long-wavelength absorption edge, even in the presence of ultrafast EET processes. Finally, the time

constant τ_4=43 ps is associated with the relaxation of the Chl red forms to the ground state. This lifetime is slower than the one retrieved in the monomers (30 ps).

The slower excited state relaxation in *S. platensis* PSI trimers with respect to monomers when P_{700} is pre-oxidized, is also confirmed by TCSPC results (Figure 1). The latter experiments discriminated two relatively long-lived components, both in the monomers and trimers, having lifetimes of ~20 – 35 ps and ~55 ps, respectively. However, whereas the first is dominant in the monomer, the second is dominant in the trimer, while they are collectively described by the slowest resolved lifetime in the 2D-DAS analysis.

In summary, from the comparison of monomeric and trimeric forms of PSI, differing both in the overall antenna dimension and in the extent of red forms, significant information can be extracted concerning its functionality:

i) it can be further confirmed that the overall excited state relaxation in PSI, irrespectively of the oligomeric state, is only weakly dependent on the redox state of P_{700}. Even in the presence of P_{700}^{+} the excited state deactivates with rate constants of about ~5 ps for bulk antenna (both monomers and trimers) and 20 – 45 ps for the red forms, which are two orders of magnitude faster than the excited state lifetime of Chl *a* in vivo (2 – 4 ns)[69,70];

ii) irrespectively of the nature of excited state quenching in the presence of P_{700}^{+} (i.e. direct quenching by the cation species, or pseudo-photochemical quenching involving eC2/eC3 Chls, accompanied by rapid recombination to the ground state), the fast relaxation can be considered as an inherent mechanism preventing the formation of long-lived excited state species that may be otherwise be responsible for light-induced damage to the system;

iii) the "pure" extension of the antenna dimension occurring upon trimerisation does not appear to result in a sizable slowing down of excited state equilibration between bulk antenna and moderately red-shifted Chl forms. Interestingly, a decrease in the fastest component of the equilibration time by up to five times is observed in the trimers (100 vs 500 fs). As the rate appears to exceed the estimated one for incoherent hopping, this behavior likely involves a coherent/strong-coupling mechanism, particularly for the ultrafast uphill transfer from the red forms;

iv) the increase in the rate of ultrafast equilibration can be related to processes occurring at the monomer-monomer interface, thereby extending the nearest-neighbor interactions, both between bulk and red forms, at the respective monomer interface. However, it cannot be ruled out that the slower dynamics in PSI monomers originates from subtle yet discernible (with sufficient spectro-temporal resolution) perturbations induced by the biochemical procedures employed, since the trimeric PSI appears to be the most abundant form of the supercomplex under natural conditions;

v) even in the presence of very efficient (downhill and uphill) EET in the trimer, the extension of the antenna bandwidth to the near-IR, represented by a Chl form centered at ≈740 nm, is sufficient to significantly slow down the overall EET dynamics, by a factor of ~1.5 – 2;

vi) the dominant relaxation of ~20 ps, observed in *S. platensis* PSI monomers, resembles the values retrieved in various cyanobacteria (monomers and trimers) having a limited red form extension[48], as well as in the core of land plants, which harbors only a limited amount of low energy spectral forms that are not very red-shifted[59]. The significant increase in lifetime to ~50 ps observed in trimers, resembles instead the value commonly reported for land-plant PSI-LHCI complexes, in which red forms are located in the complex periphery[14,40,47]. Hence, it seems clear that it is the energy of the red-most forms in PSI antenna, and not their location within the supercomplex, that governs the overall excited state relaxation;

vii) extrapolation of the results obtained when P_{700} is pre-oxidized to open conditions (P_{700} in neutral state), possible because the overall EET dynamics remains largely unperturbed, would indicate a loss of trapping efficiency of only ~ 2 % in PSI trimers with respect to monomers, with photochemical yields being larger than 0.96 in both cases.

SUPPLEMENTARY MATERIALS

1- Fluence-dependence of excited state dynamics

2- 2DES maps, excited state dynamics, over the full-time windows investigated.

3- Global analysis of the monomeric *S. platensis* PSI including the non-decaying component together with a different constrained model for comparison.

ACKNOWLEDGMENTS

SS and APC acknowledge support for this research from Fondazione Cariplo (CYAO project), grant number 2016-0667. G.C. acknowledges the support from the PRIN 2017 Project 201235SBA3-HARVEST.

AUTHOR DECLARATION

REFERENCES

1. N. Nelson, W. Junge,Annu. Rev. Biochem., **84**, 659 (2015)
2. R. Croce, H. van Amerongen, Photosynth. Res., **116**, 153 (2013)
3. S. Caffarri, T. Tibiletti, R.C. Jennings, S. Santabarbara, Curr.ProteinPept.Sci.,**15**, 296 (2014)
4. P. Fromme, P. Jordan, N. Krauß, Biochim. Biophys. Acta, Bioenerg., **1507**, 5 (2001)
5. M. Watanabe, H. Kubota, H. Wada, R. Narikawa and M. Ikeuchi, Plant Cell Physiol.,**52**, 162 (2010)
6. M. Li, D. A. Semchonok, E. J. Boekema and B. D. Bruce, Plant Cell **26**, 1230 (2014)
7. J. Kruip, P.R. Chitnis, B. Lagoutte, M. Rögner, E.J. Boekema, J. Biol. Chem., **272**, 17061 (1997)
8. J. Kruip, D. Bald, E.J. Boekema, M. Rögner, Photosynth. Res., **40**, 279 (1994)
9. V.P. Chitnis, Q. Xu, L. Yu, J.H. Golbeck, H. Nakamoto D.-L. Xie, P.R. Chitnis, J. Biol. Chem., **268**, 11678 (1993)
10. P. Jordan, P. Fromme, H.T. Witt, O. Klukas, W. Saenger, N. Krauss, Nature **411**, 909 (2001)
11. S. Santabarbara, P. Heathcote, M.C. Evans, Biochim. Biophys. Acta, **1708**, 283 (2005)

12. S. Santabarbara, L. Galuppini, A.P. Casazza, J. Integr. Plant Biol., **52**, 735 (2010)

13. B. Gobets, R. van Grondelle, Biochim. Biophys. Acta, **1057**, 80 (2001)

14. R. Croce, G. Zucchelli, F.M. Garlaschi, R.C. Jennings, Biochemistry, **37**, 17355 (1998)

15. R.C. Jennings, F.M. Garlaschi, E. Engelmann, G. Zucchelli, Febs Lett., **547**, 107 (2003)

16. R. Croce, A. Chojnicka, T. Morosinotto, J.A. Ihalainen, F. van Mourik, J.P. Dekker, R. Bassi, R. van Grondelle, Biophys. J., **93**, 2418 (2007)

17. E. Wientjes, R. Croce, Biochem. J.,**433**, 477 (2011)

18. S. Santabarbara, A.P. Casazza,E. Belgio, R. Kaňa, O. Prášil,Advances in Photosynthesis and Respiration,**45**, 261 (2020)

19. N.V. Karapetyan, E. Schlodder, R. van Grondelle, J.P. Dekker,Advances in Photosynthesis and Respiration, **24**, 177 (2006)

20. M. Rätsep, T.W. Johnson, P.R. Chitnis, J. Phys. Chem. B, **104**, 836 (2000)

21. J.M. Hayes, S. Matsuzaki, M. Rätsep, J. Phys. Chem. B, **104**, 5625 (2000)

22. V. Zazubovich, S. Matsuzaki, T.W. Johnson, J.M. Hayes, P. Chitnis, Chem. Phys., **275**, 47 (2003)

23. M. Byrdin, P. Jordan, N. Krauss, P. Fromme, D. Stehlik, E. Schlodder, Biophys J., **83**, 433 (2002)

24. A. Damjanovic, H.M. Vaswani, P. Fromme, G.R. Fleming, J. Phys. Chem. B,**106**, 10251 (2002)

25. M.K. Sener, D.Y. Lu, S.H. Park, K. Schulten, P. Fromme,Biophys. J.**82**, 292 (2002)

26. M.K. Sener, C. Jolley, A. Ben-Shem, P. Fromme, N. Nelson, R. Croce, K. Schulten,Biophys. J.,**89**, 1630 (2005)

27. M. Brecht, H. Studier, A.F. Elli, F. Jelezko, R. Bittl, Biochemistry, **46**, 799 (2007)

28. A. Khmelnitskiy, H. Toporik,Y. Mazor, R. Jankowiak, J. Phys. Chem. B, **124**, 8504 (2020)

29. H. Toporik, A. Khmelnitskiy, Z. Dobson, R. Riddle, S. Williams, S. Lin, R. Jankowiak and Y. Mazor, Nature Comm., **11**, 5279 (2020)

30. V.V. Shubin, N. V. Karapetyan, Biophysics., **31**, 18 (1986)

31. V.V. Shubin, S.D.S. Murthy, N.V. Karapetyan, P. Mohanty, BiochimBiophys. Acta,**1060**, 28 (1991)

32. V.V. Shubin, I.N. Bezsmertnaya, N.V. Karapetyan, FEBS Lett. **309**, 340 (1992)

33. V.V. Shubin, V.L. Tsuprun, I.N. Bezsmertnaya, N.V. Karapetyan, FEBS Lett. **334**, 79 (1993)

34. N.V. Karapetyan, D. Dorra, G. Schweitzer, I. N. Bezsmertnaya, A. R. Holzwarth, Biochemistry,**36**, 13830 (1997)

35. N.V. Karapetyan, A. R. Holzwarth, M. Rogner, FEBS Lett.,**460**, 395 (1999)

36. B. Koehne, H. W. Trissl, Biochemistry, **37**, 5494 (1998)

37. A. Cometta, G. Zucchelli, B.V. Karapetyan, E. Engelmann, F.M. Garlaschi, R.C. Jennings, Biophys. J.,**79**, 3235 (2000)

38. E. Schlodder, M. Cetin, M. Byrdin, I.V. Terekhova, N.V. Karapetyan,Biochimica et Biophysica Acta,**1706**, 53 (2005)

39. A. Rivadossi, G. Zucchelli, F.M. Garlaschi, R.C. Jennings, Photosynth. Res., **60**, 209 (1999)

40. R.C. Jennings, G. Zucchelli, R. Croce, F.M. Garlaschi, Biochim. Biophys. Acta, **1557**, 91 (2003)

41. E. Engelmann, G. Zucchelli, A.P. Casazza, D. Brogioli, F.M. Garlaschi, R.C. Jennings, Biochemistry,**45**, 6947 (2006)

42. R.C. Jennings, G. Zucchelli, S. Santabarbara, Biochim. Biophys. Acta **1827**, 779 (2013)

43. P. Galka, S. Santabarbara, T.T. Khuong, H. Degand, P. Morsomme, R.C. Jennings, E.J. Boekema, S. Caffarri, Plant Cell, **24**, 2963 (2012)

44. C. Le Quiniou, B. van Oort, B. Drop, I.H.M. van Stokkum, R. Croce, J. Biol. Chem.,**290**, 30587 (2015)

45. S. Santabarbara, T. Tibiletti, W. Remelli,S. Caffarri, Phys. Chem. Chem. Phys.,**19**, 9210 (2017)

46. E. Molotokaite, W. Remelli, A.P. Casazza, G. Zucchelli, D. Polli, G. Cerullo, S. Santabarbara, J. Phys. Chem. B,**121**, 9816 (2017)

47. M. Russo A.P. Casazza, G. Cerullo, S. Santabarbara, M. Maiuri, J. Phys. Chem. B,**125**, 3566 (2021)

48. B. Gobets, I.H. van Stokkum, M. Rögner, J. Kruip, E. Schlodder, N.V. Karapetyan, J.P. Dekker, R. van Grondelle, Biophys. J., **81**, 407 (2001)

49. B. Gobets, I.H.M. van Stokkum, F. van Mourik, J.P. Dekker, R. van Grondelle. Biophysical J., **85**, 3883 (2003)

50. D.A. Cherepanov, I.V. Shelaev, F.E. Gostev, M.D. Mamedov, A.A. Petrova, A.V. Aybush, V.A. Shuvalov, A.Y. Semenov, V.A. Nadtochenko, Biochim.Biophys. Acta, **1858**, 895 (2017)

51. D.A. Cherepanov, I.V. Shelaev, F.E. Gostev, M.D. Mamedov, A.A. Petrova, A.V. Aybush, V.A. Shuvalov, A.Y. Semenov, V.A. Nadtochenko, J. Phys. B Atomic Mol. Phys., **50**, 174001 (2017)

52. G.S. Schlau-Cohen, A. Ishizaki, G.R., Chem. Phys., **386**, 1 (2011)

53. E. Meneghin, D. Pedron, E. Collini, Chem. Phys.,**514**, 132 (2018)

54. P. Akhtar, C. Zhang, Z. Liu, H.S. Tan, P-H. Lambrev, Photosynth. Res. **135**, 239 (2018)

55. Y. Lee, M. Gorka, J.H. Golbeck, J.M. Anna, J. Am. Chem. Soc., **140**, 11631 (2018)

56. J.M. Anna, E.E. Ostroumov, K. Maghlaoui, J. Barber, G.D. Scholes, J. Phys. Chem. Lett., **3**, 3677 (2012)

57. P. Akhtar, I. Caspy, P.J. Nowakowski, T. Malavath, N. Nelson, H.S Tan, P.H. Lambrev, J. Am. Chem. Soc., **143**, 14601 (2021)

58. I.V. Shelaev, F.E. Gostev, M.D. Mamedov, O.M. Sarkisov, V.A. Nadtochenko, V.A. Shuvalov, A.Y. Biochim. Biophys. Acta, Bioenerg., **1797**, 1410 (2010)

59. M. Russo, V. Petropoulos, E. Molotokaite, G. Cerullo, A.P. Casazza, M. Maiuri, S. Santabarbara, Photosynth. Res.,**144**, 221 (2020)

60. J. M. Beechem, E. Gratton, M. Ameloot, J. R. Knutson, L. Brand and J. R. Lakowicz, in Topics in Fluorescence Spectroscopy. 2, Plenum Press, New York, 1991, pp. 241-305

61. M. Straume, S. Frasier-Cadoret and M. L. Johnson, in Topics of Fluorescence Spectroscopy, ed. Lakowicz, Plenum Press, New York, U.S.A., 1991, Vol. 2, pp. 177-240.

62. J. Réhault, M. Maiuri, A. Oriana, G. Cerullo, Rev. Sci. Instrum., **85**, No. 123107 (2014)

63. D. Brida, C. Manzoni, and G. Cerullo, Opt. Lett. **37**, 3027 (2012)

64. W. Giera, V.M. Ramesh, A.N. Webber, I.H.M. van Stokkum, R. van Grondelle, K. Giba-siewicz, Biochim. Biophys. Acta, **1797**, 106 (2010)

65. R. Moca,S.R. Meech, I.A. Heisler, J. Phys. Chem. B,**119**, 8623 (2015)

66. A. Volpato, L. Bolzonello, E. Meneghin, E. Collini, Opt. Express,**24**, 24773 (2016)

67. M. G. Müller, J. Niklas, W. Lubitz, A. R. Holzwarth, Biophys. J., **85**, 3899 (2003)

68. A. R. Holzwarth, M. G. Müller, J. Niklas, W. Lubitz, Biophys. J., **90**, 552 (2006)

69. T. Mar, Govindjee, G.S. Singhal, H. Merkelo, Biophysical Journal, **12**, 797 (1972)

70. G.F.W. Searle, C.J. Tredwell, Ciba Foundation Symposium 61 - Chlorophyll Organization and Energy Transfer in Photosynthesis. 1978 Feb 7-9(61):257-281

(a)

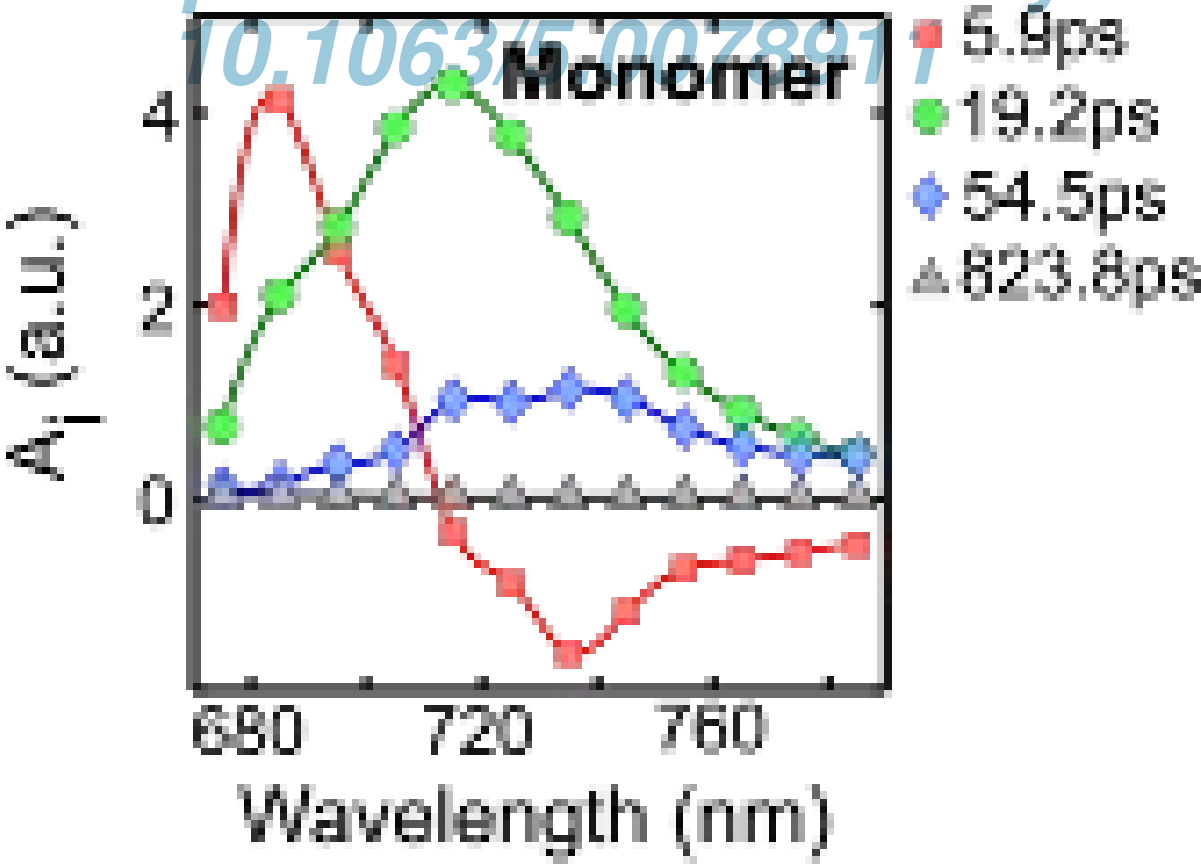

(b)